Effects of swift heavy ion-irradiation on mica- and coal-based rocks of Lower Himalayas in Sikkim, India

Archana Tiwari, Saikiran Vadavalli, Ajay Tripathi & Anand P. Pathak

Taylor & Francis
Taylor & Francis Group

Effects of swift heavy ion-irradiation on mica- and coal-based rocks of Lower Himalayas in Sikkim, India

Archana Tiwari[a], Saikiran Vadavalli[b], Ajay Tripathi[a] and Anand P. Pathak[a,b]*

[a]*Department of Physical Sciences, Sikkim University, Gangtok 737102, India;* [b]*School of Physics, University of Hyderabad, Hyderabad 500046, India*

Naturally occurring mica schist and coal sedimentary sequence in Sikkimese Himalaya were collected and investigated by two micro-techniques: scanning electron microscopy/energy dispersive spectrometry and Raman spectroscopy. They were applied to identify the constituents and the structure of the minerals before and after swift heavy ion irradiation. Vibrational data and the constituents of abundantly found mica schist and coal-based rock were acquired at room temperature and were compared with those reported for their analogues in the previous reports.

Keywords: swift heavy ions; Raman spectroscopy; SEM/EDS; schist

1. Introduction

Minerals, being limited in abundance and non-renewable, are often considered as a valuable addition to earth crust. The availability of various minerals in their rich reserves turns out to be very conducive for the growth and development of the country's economy. Indian land is enriched with resources of metallic and non-metallic minerals.

Sikkim, an Indian state in North-Eastern Himalaya, stretches its boundary up to Tibetan Plateaus in the North, the Chumbi Valley of Tibet and Bhutan in the East, Nepal in the West, and Darjeeling district of West Bengal in the South (Figure 1). Being one of the youngest range in the world, the rocks and minerals of Himalaya possess many interesting characteristics; majority of these are yet to be unearthed. East district of Sikkim, the study area for the article, is known to be dominated by mica schist, chlorite schist, sericite schist, and quartz schist (*1–5*).

Swift heavy ion (SHI) irradiation is often used to modify the molecular structure in various materials leading to changes in their chemical, electronic, and optical properties (*6, 7*). The ion irradiation induces irreversible changes in the structure of the materials and their properties. The irradiation provides several possibilities for creating extremely high-energy densities inside various material targets and matrices. SHI irradiation experiments have helped in discovering materials capable of inactivating radioactive wastes and prediction of nuclear tracks forming inside actinide-bearing minerals such as apatite and zircon (*8–13*). In addition to this, SHIs have been extensively used in lithographic techniques, especially in designing the nanostructures on the
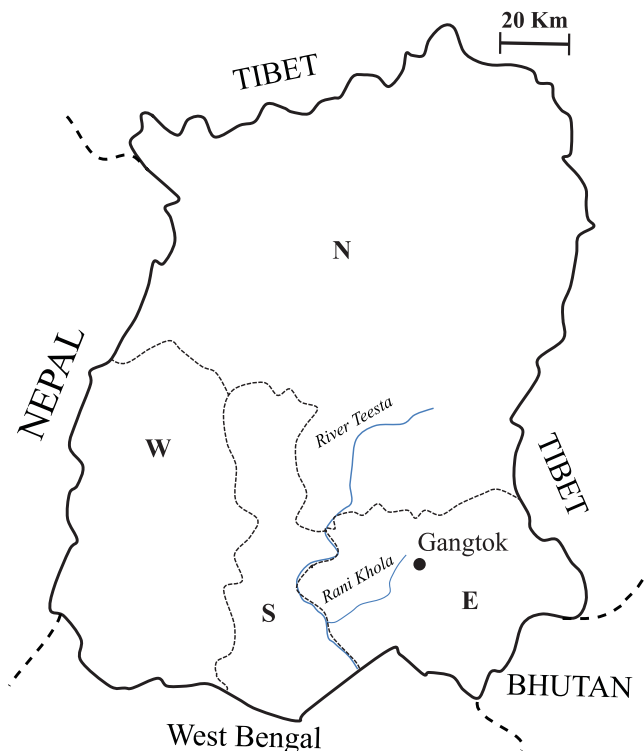

Figure 1. The geological map of Sikkim. The black curve shows the state boundary, whereas the internal black-dashed curve shows the district boundaries within Sikkim (N-North, E-East, S-South, and W-West districts). The major running rivers of the East district are also highlighted in the figure.

substrate materials (*14–18*). Mica-based materials offer both layered and nanoporous templates for interesting fabrications (*19–21*). Being cheap and abundant, mica has been widely studied under the influence of SHI irradiation (*22–25*). In this article, we have studied the effects of SHI irradiation on mica schist and coal minerals obtained from the Sikkimese Himalaya. The region is barely studied in order to evaluate the minerals' composition, and therefore the possible applications in the field of science and technology.

Scanning electron microscopy coupled with energy dispersive spectrometry (SEM/EDS) and micro-Raman spectroscopy is an efficient technique for understanding the structural and chemical modifications of materials upon the SHI irradiation. In this article, we intend to highlight the effects of SHI on the schist which not only consist of mica, but also other mineral inclusions in it. We have characterized three different rock samples before and after the irradiation. First two samples were chosen based on their close analogy to mica schist and the remaining sample is chosen as per being analogous to a coal-like mineral.

2. Materials and methods

Three samples were collected from Gangtok in East district of Sikkim. Of these three samples, two samples, namely Sample 1 and Sample 2, were pale and lustrous schist, whereas Sample 3 was black in color (Figure 2).

SHI irradiation of samples was done at room temperature with 80 MeV Ni ions from 15UD pelletron accelerator facilities available at Inter-University Accelerator Centre, New Delhi.

Figure 2. Raw samples collected from East Sikkim: (a) Sample 1, (b) Sample 2, and (c) Sample 3.

All samples were irradiated with a fluence of 10^{13} ions cm^{-2} under high vacuum $< 10^{-6}$ mbar. To avoid heating the samples, a low beam current of 1 pnA was maintained during the irradiation experiments.

Raman spectroscopy measurements were carried out at room temperature in backscattering geometry with a 785 nm diode laser beam of 30 mW power. The laser beam was focused on the sample surface using 50× objective. Raman spectra were observed using Renishaw in via spectrometer, micro-Raman (RM 2000) model. For each measurement, between 5 and 10 spectral accumulations at 10 s exposure time were recorded. The samples' surface layers were analyzed with no further preparation being undertaken. The spectral cutoff of the instrument was 100 cm^{-1}. A Lorentzian fitting in OriginPro 8 was done in order to evaluate the peak parameters.

Following the Raman analyses, the surface morphology and distribution of minerals in the samples were imaged using field emission scanning electron microscopy (FESEM); FESEM— Carl Zeiss Ultra-55 model. Qualitative elemental analyses were also carried out using an Oxford Inca EDS coupled with FESEM.

3. Results and discussion

3.1. *SEM/EDS analysis*

Figure 3 shows an SEM/EDS image of the three samples with distinct peaks for Al, Si, Mg, Au, O, K, Ti, Fe, and Ce. The gold (Au) peak is derived from the gold coating on the samples required for SEM/EDS measurements. EDS data of Samples 1–3 yield the composition which is given in Table 1.

It is observed that both Samples 1 and 2 have similar elemental contents than that of Sample 3. Sample 1 in comparison to Sample 2 has higher contents of Mg and Al, whereas the latter has higher contents of Si and K. In Sample 3, the presence of a few trace elements such as Ti, Ce, and Fe was also observed.

3.2. *Raman spectra analysis*

Raman spectra of the three samples are plotted in Figures 4–6. Most of the Raman peaks are observed in the range 100–1600 cm^{-1}. The peaks and their relative intensities are reproducible throughout the entire sample. Very few peaks are observed in the higher energy region. The peak positions of the strongest, medium, and weak intensity peaks are given in Table 2. In this section, the Raman spectra of Samples 1 and 2 are discussed first followed by that of Sample 3. Both irradiated and unirradiated samples are discussed.
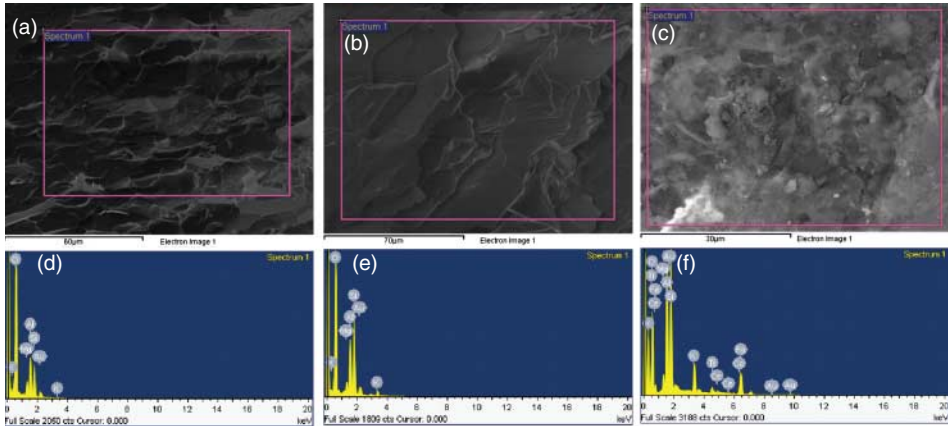
Figure 3.   SEM images of three samples: (a) Sample 1, (b) Sample 2, and (c) Sample 3. SEM/EDS spectrum of three samples: (d) Sample 1, (e) Sample 2, and (f) Sample 3.

Table 1.   Chemical composition of the samples obtained by SEM/EDS analyses.

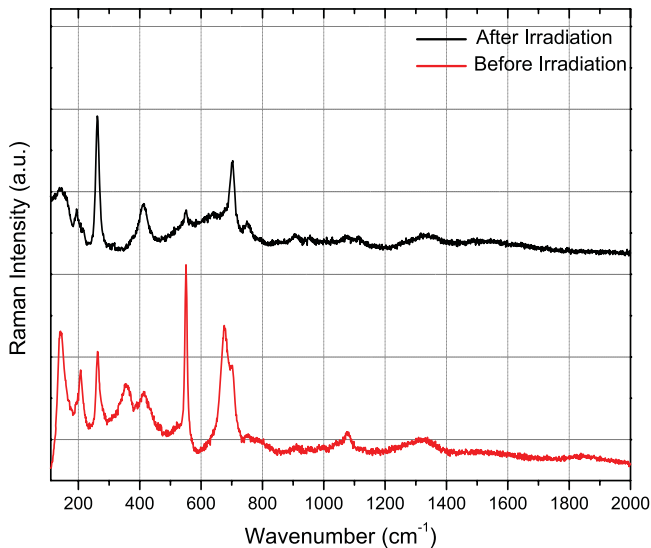| Element	Sample 1 Weight (%)	Sample 2 Weight (%)	Sample 3 Weight (%)
O	84.10	83.36	55.78
Mg	2.64	1.62	1.72
Al	6.42	5.99	13.42
Si	6.15	7.91	18.87
K	0.30	0.45	4.51
Au	0.44	0.69	0.16
Ti			0.82
Fe			4.61
Ce			0.11
Total	100	100	100

Figure 4.   Raman spectra of Sample 1 before and after the SHI irradiation in the range 100–2000 cm^{-1}.
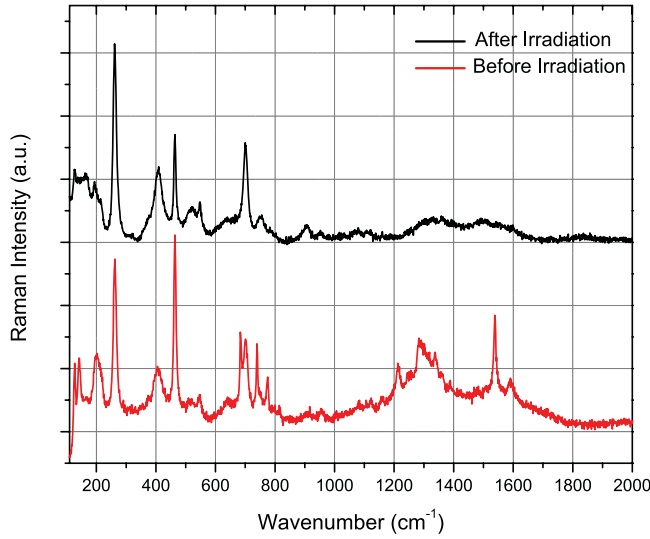
Figure 5. Raman spectra of Sample 2 before and after the SHI irradiation in the range 100–2000 cm^{-1}.
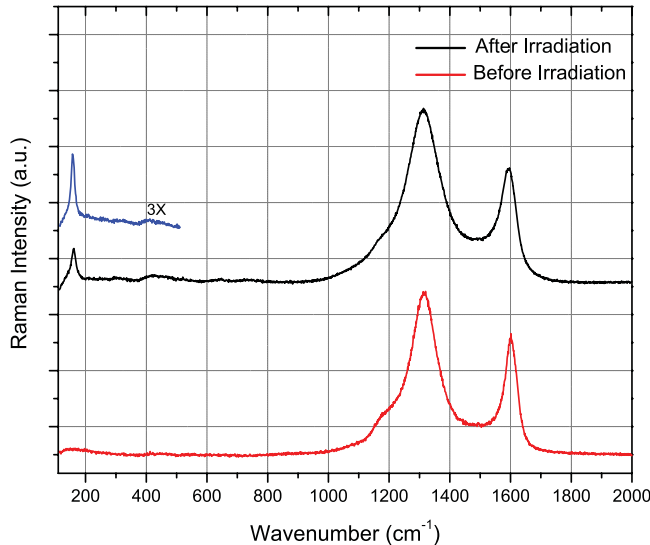

Figure 6. Raman spectra of Sample 3 before and after the SHI irradiation in the range 100–2000 cm^{-1}.

Mica minerals are composed of an octahedral sheet with (Mg, Al, etc.) cations sandwiched between two parallel tetrahedral sheets of $(Si, Al)O_4$ tetrahedra. This structure is called 2:1 layered phyllosilicate. Natural micas, *e.g.* lepidolite, muscovite, phlogopite, and margarite, are known to exhibit different Raman peaks in the 50–1250 cm^{-1} regions (*26–30*).

Spectra between 100 and 300 cm^{-1}: The peaks below 230 cm^{-1} are mainly assigned to the internal vibrations of MO_6 octahedron in both di- and tri-octahedral micas. Here, M is the octahedral cation, for example Mg^{2+} in phlogopite and Al^{3+} in muscovite (*26, 31*). These peaks are attributed to the symmetric bending modes of O−Si−O and O−Al−O groups (*32, 33*). Common peaks for both Samples 1 and 2 are found at 141, 196–203, and 262 cm^{-1}. The intense energy peak at 141 cm^{-1} is attributed to the O−Al−O symmetric bend in both samples. The presence of this

Table 2. Curve fitting data of the micro-Raman spectra of Samples 1– 3.

Sample 1		Sample 2		Sample 3	
Unirradiated	Irradiated	Unirradiated	Irradiated	Unirradiated	Irradiated
		128 (m)	128 (w)		
141 (s)	141 (w)	142 (m)	163 (w)		
205 (m)	196 (w)	203 (m)	196 (w)		
	214 (w)		214 (w)		
263 (m)	262 (s)	262 (s)	262 (s)		
350 (m)					
419 (m)	413 (m)	405 (m)	408 (m)		
		464 (s)	464 (s)		
		517 (w)	517 (w)		
551 (s)	550 (w)	547 (w)	547 (w)		
676 (s)	642 (w)	641 (w)	645 (w)		
		684 (m)			
701 (m)	701 (s)	701 (m)	701 (m)		
750 (w)	751 (w)	740 (m)	755 (w)		
		775 (m)			
	912 (w)	910 (w)	905 (w)		
		956 (w)	959 (w)		
1067 (w)	1076 (w)		1079 (w)	1177 (w)	
		1213 (w)			
		1291(w)			
1321 (w)	1327 (w)			1310 (s)	1310 (s)
		1337 (w)	1350 (w)		
		1360 (w)			
		1388 (w)			
		1507 (w)	1500 (w)		
		1538 (m)			
		1590 (w)	1597 (m)	1590 (m)	
1845 (w)					
3126 (w)	3140 (w)	3112 (w)	3072 (w)	2570 (w)	2590(w)
3626 (w)	3612 (w)	3250 (w)	3605 (w)	2958 (w)	3021 (w)

Note: Strong (s), medium (m), and weak (w) Raman peaks are indicated with s, m, and w, respectively.

peak is attributed to the Kaolinite mineral in the schist samples. The evidence of $128\,cm^{-1}$ peak in Sample 2, attributed to O−Si−O symmetric bend, further affirms the presence of the Kaolinite mineral in this sample. The narrow line-width of $141\,cm^{-1}$ peak in Sample 2 as compared to that of Sample 1 shows more ordered Kaolinite in Sample 2 than in Sample 1. Farmer and Ishii et al. also reported the presence of $128\,cm^{-1}$ peak to the vibrations of hexagonal Si_2O_5 layer. The higher energy ($141\,cm^{-1}$) is attributed to O−Al−O symmetric bend of the AlO_6 group of Kaolinite and the lower energy peak ($128\,cm^{-1}$) is attributed to that of O−Si−O symmetric bend (*34–36*). The large intensity of these peaks occurs as a result of a vibrational mode which induces significant change in the polarizability. The change in the peak positions and in the widths are, therefore, related to the stress on the Kaolinite crystal structure.

The $196\,cm^{-1}$ peak is strong in dioctahedral micas. This wavenumber increases if the concentration of Al ion increases inside the mica schist. The $262\,cm^{-1}$ peak intensity is strong in all dioctahedral micas and trilithionite, whereas it is weak in compositions closer to phlogopite (*31*). It is observed that in both Samples 1 and 2, the intensity of $\sim 260\,cm^{-1}$ peak is medium to strong. This peak occurs in those dioctahedral micas where the octahedral sites either have Al^{3+} impurities or have no identical cations (*26*, *31*).

Interestingly, we have observed that the Raman peaks in this region change enormously upon the SHI irradiation. In these samples, 128, 141, and $196–203\,cm^{-1}$ peaks intensities and FWHM changes upon the irradiation. More commonly, the intensity decreases, whereas the

width gets broader. The $128\,\text{cm}^{-1}$ peak becomes weaker and broader after the irradiation. The peak width changes from 16 to $34\,\text{cm}^{-1}$. Analogous to this, peak positioned at $141\,\text{cm}^{-1}$ also gets weaker and broader. It can be deduced from here that O−Al−O and O−Si−O symmetric bends are distorted upon SHI leading to broad widths and poor intensities. On the contrary, the peak intensity at $262\,\text{cm}^{-1}$ in Sample 1 increases upon the irradiation, whereas the peak width becomes narrower; the FWHM changes from 16 to $12\,\text{cm}^{-1}$. The changes in $262\,\text{cm}^{-1}$ peak in Sample 1 are attributed to the restricted stretching modes of O−Al−O and O−Si−O upon the SHI irradiation. Also, few weak peaks are seen emerging and disappearing in the range $196–203\,\text{cm}^{-1}$.

Spectra between 300 and 1600 cm^{-1}: In previous reports, the peaks in the higher wavenumber region are assigned to the vibrations of Si_2O_5 layers, internal vibrations of distorted SiO_4 tetrahedron, vibrations of Si−O−Si, Si−O−Al, Al−O−Al, Si−O, Al−O, and Al−O−H (*37–39*). The characteristic quartz peaks at 355 and $464\,\text{cm}^{-1}$, attributing to O−Si−O deformation and Si−O stretching mode, respectively, are observed in the spectra of Samples 1 and 2. This reveals that these samples have inclusions of quartz composition (*30, 40–42*).

Sample 1 also exhibits a strong peak at $550\,\text{cm}^{-1}$. This peak is attributed to Si−O−Si and O−Si−O bending modes in SiO_4 tetrahedron. A broad peak at $419\,\text{cm}^{-1}$ in the sample is known to occur in dioctahedral micas and trilithionite due to the convolution of O−H liberation and Si−O vibrations (*26, 31*). Also, most of the Al-bearing silicates show a strong but wide peak at $420\,\text{cm}^{-1}$ (*e.g.* muscovite and montmorillonite), whereas Mg-bearing silicates show a strong peak at $350\,\text{cm}^{-1}$ (*e.g.* serpentine, phlogopite, and chlorite). We report the presence of both peaks in Samples 1 and 2 pertaining to the presence of Al and Mg in their composition.

Si−O−Si vibrations are also related to two more peaks at 679 and $702\,\text{cm}^{-1}$ in phlogopite and muscovites. Both peaks are due to symmetric stretching of the bridging oxygen. Amongst the reported spectra, both Samples 1 and 2 show peaks at ~672 and $\sim701\,\text{cm}^{-1}$. Tilli et al. (*31, 43, 44*) reported that if $700\,\text{cm}^{-1}$ peak, attributed to Al−O−Al and Si−O−Si bending vibrations, lies at slightly higher wavenumbers, this could be due to the presence of dioctahedral K–micas in the sample.

The peaks in the $950–1150\,\text{cm}^{-1}$ are attributed to the stretching Si−O−Si or Si−O−Al modes, whereas the peaks in the $740–900\,\text{cm}^{-1}$ arise due to the octahedral Al−O and Al−O−Al stretching modes (*45*). The most intense peaks in $500–750\,\text{cm}^{-1}$ spectral region are attributed to the Si−O−Si stretching vibrations, whereas the bands originating from the translational Mg(Al)−O modes give rise to the strong peaks in the lower wavenumber region. The Raman peaks at 550 and $750\,\text{cm}^{-1}$ are together attributed to Si−O−Si vibrations in the schist. While looking for these peaks in the observed spectra, we found that in Sample 1, the peaks are observed at 551 and $750\,\text{cm}^{-1}$, whereas for Sample 2 peaks are found at 547 and $740\,\text{cm}^{-1}$. The spectra also show the presence of weak and broad peaks in the range $1000–2000\,\text{cm}^{-1}$ which are attributed to antisymmetric stretching modes of bridging oxygen, Si−O−Si. The interpretation is that $1075\,\text{cm}^{-1}$ peak arises due to symmetric stretch from an $Si_2O_5^{2-}$ unit in both samples (*44–48*).

Upon the irradiation, the peaks at 550 and $676\,\text{cm}^{-1}$ in Sample 1 and $740\,\text{cm}^{-1}$ in Sample 2 become weaker and broader. The FWHM for these peaks increases approximately three times upon the irradiation. The broadening of these peaks affirms the distortion in the Si(Al)−O−Al(Si) vibrations upon SHI (*45*). This can also be attributed to large tetrahedral Si/Al disorder in the silicate structures arising from the tetrahedral O−Si(Al)−O bending vibrations (*49*). On the contrary, the peak intensity at $701\,\text{cm}^{-1}$ in Sample 1 increases upon the irradiation and the peak width changes from 23 to $19\,\text{cm}^{-1}$. This phenomenon reveals an ordering in the bridging oxygen; Si−O−Si vibration after the SHI irradiation (*40*).

Raman spectroscopy has been extensively used to distinguish graphite, graphene, and other carbon allotropes such as coal and char. In coal-based minerals, both G and D bands are evidently found (*50, 51*). When compared with our Sample 3, all Raman features resembled to those reported

for the coal and disorder graphite. Three reproducible peaks are found in Sample 3. The G band (graphitic band) is found centered at $\sim$1590 cm^{-1}. It mainly represents the aromatic ring quadrant breathing ([52], [53]). The D band (disordered band) which is observed at $\sim$1310 cm^{-1} arises due to aromatic structures with more than six rings. The S band, centered at $\sim$1180 cm^{-1}, which occurs as a shoulder of D band, tentatively represents sp^2–sp^3 bonds or C−C and C=C stretching vibrations of polyene-like structures ([54]).

In Sample 3, the relative peak intensities remain unchanged for G and D bands after the irradiation. However, they get broader from 120 to 185 cm^{-1} for G band, and 53 to 69 cm^{-1} for D band upon the irradiation. In addition to these peaks, a new peak is observed after the irradiation in the lower wavenumber region. In the spectrum of the SHI-irradiated sample, a narrow peak at $\sim$150 cm^{-1} with a width of 15 cm^{-1} is observed. In the literature, the peaks in the lower wavenumber region are attributed to radial breathing modes (RBM) of carbon nanotubes (CNTs) that reflect both tube diameters and is indicative of single versus multi-walled structures in carbon polymorph ([55], [56]). The peaks with smaller RBM frequencies correspond to larger diameter tubes. In this work, we were only be able to locate 150 cm^{-1} peak after the irradiation. However, this peak is not found uniformly reproducible over the surface of the sample. Similar works have been done in this direction, where graphite and coal have been used to synthesize empty fullerene and onion-like fullerene molecules ([57–60]).

4.   Conclusions

We have studied the effects of the irradiation by Ni SHIs with energy 80 MeV, on the naturally occurring rock samples, namely mica schist and coal originated from the Sikkimese Himalaya. The pristine and irradiated samples were investigated using Raman spectroscopy and SEM/EDS. Our study reveals the presence of di-octahedral mica in both schist samples. They also consist of Kaolinite clay mineral and quartz inclusions.

This study reveals that all samples undergo structural modifications. While the positions of most of the Raman peaks remain constant, they show distinct broadening of the full width at half maxima. This demonstrates poor short-range order of the crystal structure upon the irradiation and could also be an indicator for amorphization. For instance, in Samples 1 and 2, the changes in Raman peaks in the lower frequency region are attributed to the distortion of O−Al−O and O−Si−O symmetric bends upon SHI which leads to broad line-widths and poor intensities. The change in 262 cm^{-1} peak illustrates restricted translations due to these distorted bending modes. Also, in the higher frequency region, the broadening of the peaks affirms the distortion in the Si−O−Si vibrational modes in the samples. This has been further attributed to large tetrahedral Si/Al disorder in the silicate structures arising from O−Si(Al)−O bending vibrations.

For coal mineral, the Raman results were studied primarily through the modification of D and G peaks. The behavior of these peaks shows that at the ion fluence of 10^{13} ion cm^{-2}, the peaks get broader and a new peak emerges at $\sim$150 cm^{-1}. This can be attributed to the formation of CNTs on the surface of coal mineral upon the SHI irradiation. It is apparent that broadening of D and G bands is an indication of amorphization in the system.

It is required to understand how the defects are being produced in the layered silicates with multiple inclusions such as quartz and clay minerals. The findings can be utilized for the fabrications of variety of nanoterrace materials with multiple stacks having sharp edges and also to look in to the potential applications of these readily available minerals. From the present study, we are encouraged to further extend this work of the SHI irradiation on such coal and graphite samples in order to synthesize various kinds of carbon nanomaterials.

Acknowledgement

References

(1) Bhasin, R.; Grimstad, E.; Larsen, J.O.; Dhawan, A.K.; Singh, R.; Verma, S.; et al. *Eng. Geol.* **2002,** *64* (4), 351–368.
(2) Sharma, N.; Pradhan, S.; Arrawatia, M.L.; et al. Lake 2010: Wetlands, Biodiversity and Climate Change, 2010, pp 1–10.
(3) Acharyya, S.K. *J. Geol. Soc. India* **1989,** *22,* 5.
(4) Ghosh, A.K. *Econ. Geol.* **1968,** *63,* 682.
(5) Ghosh, S. *Introducing Geography 2*, 2nd ed.; Pearson Education India, 2008.
(6) Singh, J.; Singhm, R.; Ghosh, S.; Tripathi, A.; Kabiraj, D.; Gupta, S.; Som, T.; Kumar, R.; Arora, S.; Asokan, K.; Avasthi, D.; Kanjilal, D.; Mishra, N.; et al. *Nucl. Instrum. Methods Phys. Res., Sect. B* **1999,** *156,* 206–211.
(7) Bouffard, S.; Gervais, B.; Leroy, C. *Nucl. Instrum. Methods Phys. Res., Sect. B* **1995,** *105,* 1–4.
(8) Weikusat, C.; Miletich, R.; Glasmacher, U.; Trautmann, C.; et al. *Phys. Chem. Miner.* **2010,** *37,* 417–424.
(9) Weikusat, C.; Glasmacher, U.; Schuster, B.; Trautmann, C.; Miletich, R.; et al. *Phys. Chem. Miner.* **2011,** *38,* 293–303.
(10) Ewing, R.C. *Mineral. Mag.* **2011,** *75* (4), 2359–2377.
(11) Fourdrin, C.; Allard, T.; Monnet, I.; Menguy, N.; Benedetti, M.; et al. *Environ. Sci. Technol.* **2010,** *44* (7), 2509–2514.
(12) Garrido, F.; Gentils, A.; Thomé, L. *Surf. Coat. Technol.* **2005,** *196* (1–3), 63–68.
(13) Thomé, L.; Garrido, F. *Vacuum* **2001,** *63* (4), 619–626.
(14) Sanz, R.; Jensen, J.; Johansson, A.; Skupinski, M.; Possnert, G.; Boman, M.; Hernandez-Vélez, M.; Vazquez, M.; et al. *Nanotechnology* **2007,** *18* (30), 305303.
(15) Sanz, R.; Jaafar, M.; Hernández-Vélez, M.; Asenjo, A.; Vázquez, M.; et al. *Nanotechnology* **2010,** *21* (23), 235301.
(16) Toulemonde, M.; Trautmann, C.; Balanzat, E.; Hjort, K.; et al. *Nucl. Instrum. Methods Phys. Res., Sect. B* **2004,** *216* (0), 1–8.
(17) Aumayr, F.; El-Said, A.; Meissl, W. *Nucl. Instrum. Methods Phys. Res., Sect. B* **2008,** *266* (12–13), 2729–2735.
(18) Itoh, N.; Duffy, D.M.; Khakshouri, S.; et al. *J. Phys. Condens. Matter* **2009,** *21* (47), 474205.
(19) Sun, L.; Chien, C.; Searson, P. *J. Mater. Sci.* **2000,** *35,* 1097–1103.
(20) Fink, D.; Chadderton, L. *Radiat. Eff. Def. Solids* **2005,** *160* (3–4), 67–83.
(21) Lang, M.; Glasmacher, U.; Moine, B.; Neumann, R.; et al. *Nucl. Instrum. Methods Phys. Res., Sect. B* **2004,** *218* (0), 466–471.
(22) Singh, M.; Kaur, N.; Singh, L. *Nucl. Instrum. Methods Phys. Res., Sect. B* **2010,** *268* (17–18), 2617–2625.
(23) Khan, E.; Waheed, A.; Tahseen, R.; Qureshi, I.; Khan, H.; Matiullah; et al. *Int. J. Radiat. Appl. Instrum. Part D. Nucl. Tracks Radiat. Meas.* **1991,** *19* (1–4), 629–630.
(24) Singh, M.; Kaur, N.; Singh, L. *Radiat. Phys. Chem.* **2010,** *79* (12), 1180–1188.
(25) Thibaudau, F.; Cousty, J.; Balanzat, E.; et al. *Phys. Rev. Lett.* **1991,** *67,* 1582–1585.
(26) Loh, E. Optical vibrations in sheet silicates. *J . Phys. C: Solid State Phys.* **1973,** *6,* 1091.
(27) Clemens, J.; Circone, S.; Navrotsky, A.; et al. *Geochim. Cosmochim. Acta* **1987,** *51,* 2569.
(28) McKeown, D.; Bell, M.; Kim, C. *Phys. Rev. B* **1993,** *48,* 16357.
(29) McKeown, D.; Bell, M.; et al. *Phys. Chem. Miner.* **1995,** *22,* 137.
(30) Sharma, S.; Mammone, J.; et al. *Nature* **1981,** *292,* 140.
(31) Tlili, A.; Smith, D.C.; Beny, J.M.; et al. *Mineral. Mag.* **1989,** *53,* 165.
(32) Blaha, J.; Rosasco, G. *Anal. Chem.* **1978,** *50,* 892–896.
(33) Rosasco, G.; Blaha, J. *Appl. Spectrosc.* **1980,** *34,* 140–144.
(34) Farmer, V.; Velde, B. *Mineral. Mag.* **1973,** *39,* 282–288.
(35) Ishii, M.; Shimanouchi, T.; Nakahira, M. *Inorg. Chim. Acta* **1967,** *1,* 387–392.
(36) Farmer, V. *The Layer Silicates*, Mineralogical Society: London, 1974.
(37) Dutta, P.; Rao, K.; Park, J. *J. Phys. Chem.* **1991,** *95,* 6654.
(38) McMillan, P.F.; Wolf, G.H. In *Structure Dynamics and Properties of Silica Melts*; Stebbins, J.F.; McMillan, P.F.; Dingwell, D.B., Eds.; Reviews in Mineralogy Vol. 32, 1995.
(39) Ryskin, Y. *The Vibrations of Protons in Minerals*, Mineralogical Society: London, 1974.
(40) Wopenka, B.; Popelka, R.; Pasteris, J.D.; et al. *Appl. Spectrosc.* **2002,** *56* (10), 1320.
(41) Kingma, K.J.; Hemley, R.J. *Am. Mineral.* **1994,** *79,* 269.
(42) Rossman, G.R. *Rev. Mineral. Geochem.* **1984,** *13,* 145.
(43) Sen, N.; Thorpe, M.F. *Phys. Rev. B* **1977,** *15,* 4030.
(44) Mysen, B.O.; Finger, L.W.; Virgo, D.; et al. *Am. Mineral.* **1982,** *67,* 686.
(45) Langer, K.; Chatterjee, N.D.; Abraham, K. *Neues Jahrb. Mineral. Abh.* **1981,** *142,* 91–110.
(46) Brawer, S.A. *Phys. Rev. B* **1975,** *11,* 3173.
(47) Furukawa, T.; Fox, K.E.; White, W.B. *J. Chem. Phys.* **1981,** *75,* 3226.
(48) Mysen, B.O.; Virgo, D.; et al. *Am. Mineral.* **1980,** *65,* 690.

(49) McKeown, D.; Bell, M.; Etz, E. *Am. Mineral.* **1999,** *84,* 970–976.

(50) Tuinstra, F.; Koenig, J.L. *J. Chem. Phys.* **1970,** *53,* 1126–1130.

(51) Tsu, R.; H., J.G.; C., I.H.; et al. *Solid State Commun.* **1977,** *24* (12), 809–812.

(52) Li, X.; Hayashib, J.; Li, C.Z. *Fuel* **2006,** *86,* 1509–1517.

(53) Li, C.Z. *Fuel* **2007,** *86,* 1664–1683.

(54) Nemanich, R.J.; Solin, S.A. *Phys. Rev. B* **1979,** *20,* 392–401.

(55) Hulman, M.; Skákalová, V.; Krasheninnikov, A.V.; et al. *Appl. Phys. Lett.* **2009,** *94,* 071907(1–3).

(56) Antunes, E.; Lobo, A.; Corat, E.; V.J.; et al. *Carbon* **2007,** *45,* 913–921.

(57) Chadderton, L.T.; Fink, D.; MöCkel, H.J.; Dwivedi, K.K.; et al. *Radiat. Eff. Def. Solids* **1993,** *127* (2), 163–168.

(58) Gamaly, E.G.; Chadderton, L.T. *Proc. R. Soc. London, Ser. A* **1995,** *449* (1936), 381–410.

(59) Du, A.B.; Liu, X.G.; Fu, D.J.; Han, P.D.; et al. *Fuel* **2007,** *86* (1–2), 294–298.

(60) Fu, D.; Liu, X.; Lin, X.; Li, T.; Jia, H.; et al. *J. Mater. Sci.* **2007,** *42,* 3805–3809.